Geophysical Research Letters

RESEARCH LETTER
10.1029/2024GL109836

# Electrical Resistivity Changes During Heating Experiments Unravel Heterogeneous Thermal-Hydrological-Mechanical Processes in Salt Formations

**Hang Chen[1], Jiannan Wang[1], Linqing Luo[1], Shawn Otto[2], Jon Davis[2], Kristopher L. Kuhlman[3], and Yuxin Wu[1]**

[1]Lawrence Berkeley National Laboratory, Berkeley, CA, USA, [2]Los Alamos National Laboratory, Los Alamos, NM, USA, [3]Sandia National Laboratories, Albuquerque, NM, USA

**Key Points:**

- We employ 4D electrical resistivity tomography (ERT) monitoring during a controlled heating experiment in salt formations
- The resistivity data exhibits contrasting trends throughout and post-heating, indicating the heterogeneous thermal-hydrological-mechanical processes in rock salt are likely linked to the different levels of excavation damages
- Employing time-series clustering technology enables quantification and spatial distributions of excavation damage/disturbed zones within the salt formations which may help further improve the parameterization of long-term predictive models

**Supporting Information:**

Supporting Information may be found in the online version of this article.

**Correspondence to:**

H. Chen,
HChen8@lbl.gov

**Citation:**

Chen, H., Wang, J., Luo, L., Otto, S., Davis, J., Kuhlman, K. L., & Wu, Y. (2024). Electrical resistivity changes during heating experiments unravel heterogeneous thermal-hydrological-mechanical processes in salt formations. *Geophysical Research Letters*, *51*, e2024GL109836. https://doi.org/10.1029/2024GL109836

Received 16 APR 2024
Accepted 11 JUL 2024

**Author Contributions:**

**Conceptualization:** Hang Chen, Kristopher L. Kuhlman, Yuxin Wu
**Data curation:** Yuxin Wu
**Formal analysis:** Hang Chen, Jiannan Wang, Linqing Luo, Shawn Otto, Jon Davis, Kristopher L. Kuhlman, Yuxin Wu



**Abstract** Rock salt is considered a suitable medium for the permanent disposal of heat-generating radioactive waste due to its isolation properties. However, excavation damage and heating induce complex and heterogeneous thermal-hydrological-mechanical (THM) processes across different zones. Quantifying this heterogeneity is crucial for accurate long-term performance assessment models, but traditional methods lack the necessary resolution. This study employs 4D electrical resistivity tomography (ERT) monitoring during controlled heating experiments in a salt formation to unravel the spatiotemporal dynamics of THM processes. Advanced time-lapse inversion and clustering analysis quantify subsurface properties and map the heterogeneity of THM dynamics. The ERT results can estimate subsurface properties and delineate the damaged and intact zones, enabling appropriate parameterization and representation of processes for long-term modeling. This approach may be used in further improving the predictive models and ensuring the safe long-term disposal of radioactive waste in rock salt.

**Plain Language Summary** Rock salt is great for the disposal of heat-generating radioactive waste because it prevents releasing harmful radiation into the environment. However, mining and heating can cause complex changes in temperature, water flow, and pressure, affecting rock salt in various ways. It is important to understand these changes accurately for planning how the disposal will affect the rock salt, but the traditional ways of studying them are not detailed enough. In this study, we used a special technique called 4D ERT while heating up the rock salt to see how these changes happen over time and space. We analyzed the data in advanced ways to measure the underground properties and understand the complex changes. The information can improve how we model and plan the disposal of heat-generating waste. This new insight makes it easier to ensure that storing heat-generating radioactive waste in rock salt is safe for a long time.

## 1. Introduction

Nuclear power currently provides 11% of the world's electricity supply and is viewed as a critical baseload low-carbon energy source to help mitigate global climate change (Mathew, 2022). However, safe management of heat-generating radioactive waste remains a challenge for the widespread adoption of nuclear energy. If not properly isolated, some components of heat-generating radioactive waste can pose serious risks for thousands of years (Schröder et al., 2016). Deep underground geological disposal has been internationally accepted as the preferred method for long-term nuclear waste disposal, including for heat-generating radioactive waste (Birkholzer et al., 2012). Rock salt formations are considered a candidate medium for the disposal of heat-generating radioactive waste due to key attributes such as extremely low permeability and porosity, high thermal conductivity, and the ability to heal fractures (K. L. Kuhlman & Malama, 2013; Sweet & McCreight, 1983).

Understanding rock salt behavior after excavation and subsequent heat-generating radioactive waste heating is crucial for modeling repository long-term ($10^4$–$10^6$ years) safety (Hu et al., 2021; K. L. Kuhlman & Malama, 2013; K. L. Kuhlman et al., 2017). Long-term performance assessment modeling relies on accurately representing complex processes and initial condition parameterization (K. L. Kuhlman et al., 2017; Wang et al., 2023). However, subsurface processes and properties become heterogeneous due to excavation damage (Blanco-Martín et al., 2018). Three distinct zones exist: the excavation damage zone (EDZ) where salt is damaged changing properties/energy state, the excavation disturbed zone (EdZ) with altered mechanical properties but maintaining integrity, and the relatively intact far-field (K. Kuhlman et al., 2021; Tsang et al., 2005). Physical processes,

**Funding acquisition:** Kristopher L. Kuhlman, Yuxin Wu
**Investigation:** Hang Chen, Jiannan Wang, Linqing Luo, Shawn Otto, Jon Davis, Kristopher L. Kuhlman, Yuxin Wu
**Methodology:** Hang Chen, Yuxin Wu
**Resources:** Yuxin Wu
**Software:** Hang Chen
**Supervision:** Yuxin Wu
**Validation:** Hang Chen
**Visualization:** Hang Chen, Jiannan Wang
**Writing – original draft:** Hang Chen
**Writing – review & editing:** Hang Chen, Kristopher L. Kuhlman, Yuxin Wu

especially thermal-hydrological-mechanical (THM) responses and modeling focus differ across zones (Blanco-Martín et al., 2018). Physical properties such as porosity and saturation may also vary. Accurately representing variable EDZ, EdZ and far-field dynamics is vital for long-term modeling over million-year timescales. While lab-scale tests have explored THM processes (e.g., Günther et al., 2015), field-scale investigation of zone heterogeneity remains limited due to spatiotemporal resolution constraints in traditional experiments (e.g., Cosenza et al., 1999).

Geophysical methods can provide valuable spatiotemporal subsurface information across scales from sub-meter to kilometers (Binley et al., 2015), enabling imaging of heterogeneous physical properties. Among these methods, ERT, being sensitive to permeability, brine content, and rock temperature, shows promise for mapping THM processes (Hayley et al., 2007; Yaramanci, 1994). While ERT has been applied to assess the safety of the rock salt repository at the Asse salt mine (Kruschwitz & Yaramanci, 2004; Yaramanci, 2000), these studies primarily focused on hydrologic processes and water-induced mechanical processes due to the lack of thermal processes at that field research site. At the Waste Isolation Pilot Plant (WIPP) (McTigue & Nowak, 1987), controlled heating experiments were conducted in salt formations, including the Brine Availability Tests in Salt Phase 2 (BATS2) experiments following the initial BATS test (K. Kuhlman et al., 2021, 2023; Wang et al., 2023). 4D ERT monitoring was performed to study the spatial and temporal dynamics of the salt formations near the heat source during BATS2. This experiment provides a unique opportunity to link resistivity properties to integrated THM processes and properties in heated salt formations.

By combining ERT and controlled heating experiments in salt formations, this study aims to provide insights into two questions: (a) Can the ERT tool provide sufficient spatial resolution to characterize subsurface properties, thus aiding in the parameterization of initial conditions for long-term monitoring? (b) Can spatial distributions and temporal changes in resistivity provide insights into heterogeneous THM processes in rock salt formations and thus improve the representation of physical processes in long-term predictive models? In this study, we utilize advanced time-lapse inversion algorithms and time-series clustering techniques, which may further enhance the capability of ERT for safety assessments. The experiment setup and methods employed here can serve as a framework to inform other deep geologic repository tests and can also be applied in future practical geologic disposal monitoring efforts. To our knowledge, this is the first study to monitor heterogeneous THM processes in rock salt formations during a controlled heating experiment at high spatiotemporal resolutions using electrical resistivity data.

## 2. Experiments and Methods

### 2.1. Research Site

Following the first phase of the BATS experiment, another controlled heating experiment in salt formations called the BATS2 experiments, was conducted at the WIPP underground facility in New Mexico. The WIPP repository is located within the 600-m-thick Permian Salado Formation. The BATS2 experiment was carried out at a depth of 650 m below the surface (Figure 1a). In preparation for the BATS experiments, core samples were collected from the Salado Formation, which is part of the upper Permian formation of the Delaware basin (Horvorka, 1997). Analysis of the core samples revealed that the cores consist primarily of crystalline halite, with minor amounts of disseminated clay and polyhalite. Additionally, the cores were found to be highly fractured, mostly created during coring, and exhibited mineralogical variations (Betters et al., 2020).

### 2.2. Experiment Setup

During the BATS2 experiment, a comprehensive monitoring and characterization plan was implemented, including thermocouples, ERT, distributed fiber sensors, acoustic emission sensors, mechanical deformation sensors, gas chemistry analysis, and brine sampling/quantification (e.g., Figures 1a and 1b). The experimental plots were set up from the drift wall (Figure 1a) by drilling mostly horizontal boreholes, with a slight downward slant, for the heater and other measurement instruments, as shown in Figure 1b. Only the ERT results will be discussed here, and the schematic diagram of the relevant borehole layout is shown in Figure 1c. The central heater borehole (red cylinder in Figure 1c) is surrounded by four parallel ERT boreholes. A 1250-W quartz lamp infrared heater with a diameter of 12 cm and a total length of 100 cm was installed in the heater borehole. Within the heater borehole, four thermocouples (TC1 to TC4) were positioned at depths of 247, 281, 311, and 348 cm, respectively, to monitor temperatures. The four 580-cm-long ERT boreholes (blue cylinders) are located

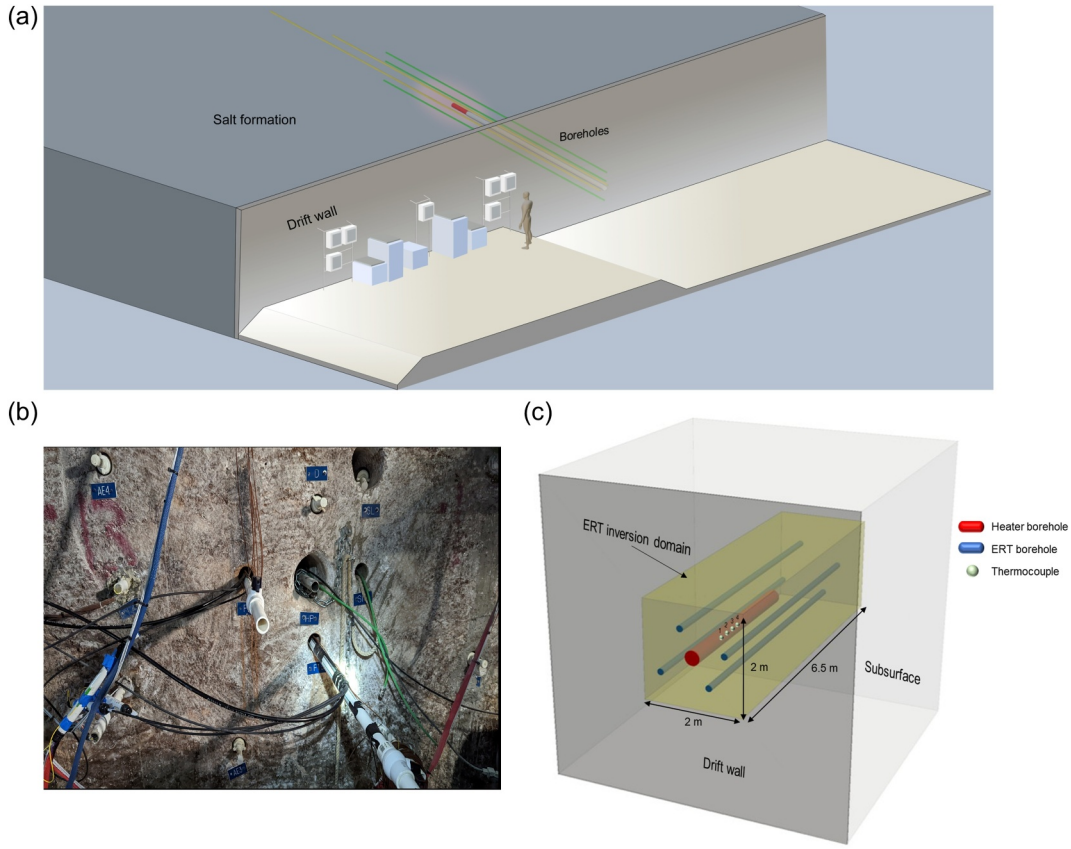


**Figure 1.** Illustration of BATS2 experimental setup: (a) a simplified schematic diagram of the drift and horizontal boreholes in the BATS2 experiment at Waste Isolation Pilot Plant, showing only the heater (red), electrical resistivity tomography (ERT) (green) and fiber optic (orange) boreholes, (b) a photograph of the field borehole setup in the BATS2 experiment, and (c) a schematic diagram of the ERT borehole setup and inversion setup in the BATS2 experiment (Z coordinate is horizontal, parallel to boreholes). In panel (c), only ERT and heater boreholes discussed in this paper are presented.

approximately 75 cm from the heater borehole and drift wall. Each ERT borehole contains 16 copper-ring electrodes spaced approximately 30 cm apart and distributed from 120 to 580 cm depth. The electrodes were controlled by an ERT data acquisition system from Multi-Phase Technologies (MPT DAS-1), located in a circulation-filtered enclosure within the drift to minimize corrosion effects from salt dust.

The first four heating phases during the BATS2 experiment are shown in Figure 2a. The first heating phase started in late July 2022 and lasted for three weeks, maintaining a temperature of 60°C, followed by a 2-week cooling period. After the initial cooling phase, the second heating phase began, lasting 3 weeks with a temperature of 80°C, and then another 2-week cooling period. Similarly, the third heating phase started after the second cooling phase, maintaining a temperature of 100°C. The initial attempt of the fourth heating phase experienced a failure shortly after the third cooling phase. The second attempt of the fourth heating phase eventually started at the beginning of March 2023 and continued for three weeks at a temperature of 130°C.

### 2.3. Electrical Resistivity Tomography Data Process and Inversion

The ERT monitoring data was collected daily from March 2022 to October 2023, utilizing a four-electrode setup with two electrodes injecting current into the salt formation and two measuring the resulting electrical potential. An optimized survey design following Wilkinson et al. (2006) achieved high resolution, spatial coverage, and reduced acquisition time, resulting in 3,072 daily resistance measurements. Overall, BATS2 ERT data quality was good, with stack errors mostly below 20 Ω and contact resistance below 3,000 Ω, allowing preliminary analysis of raw resistance trends. Data filtering was necessary before inversion to eliminate outliers with unusually high or low values and ensure reliable results.

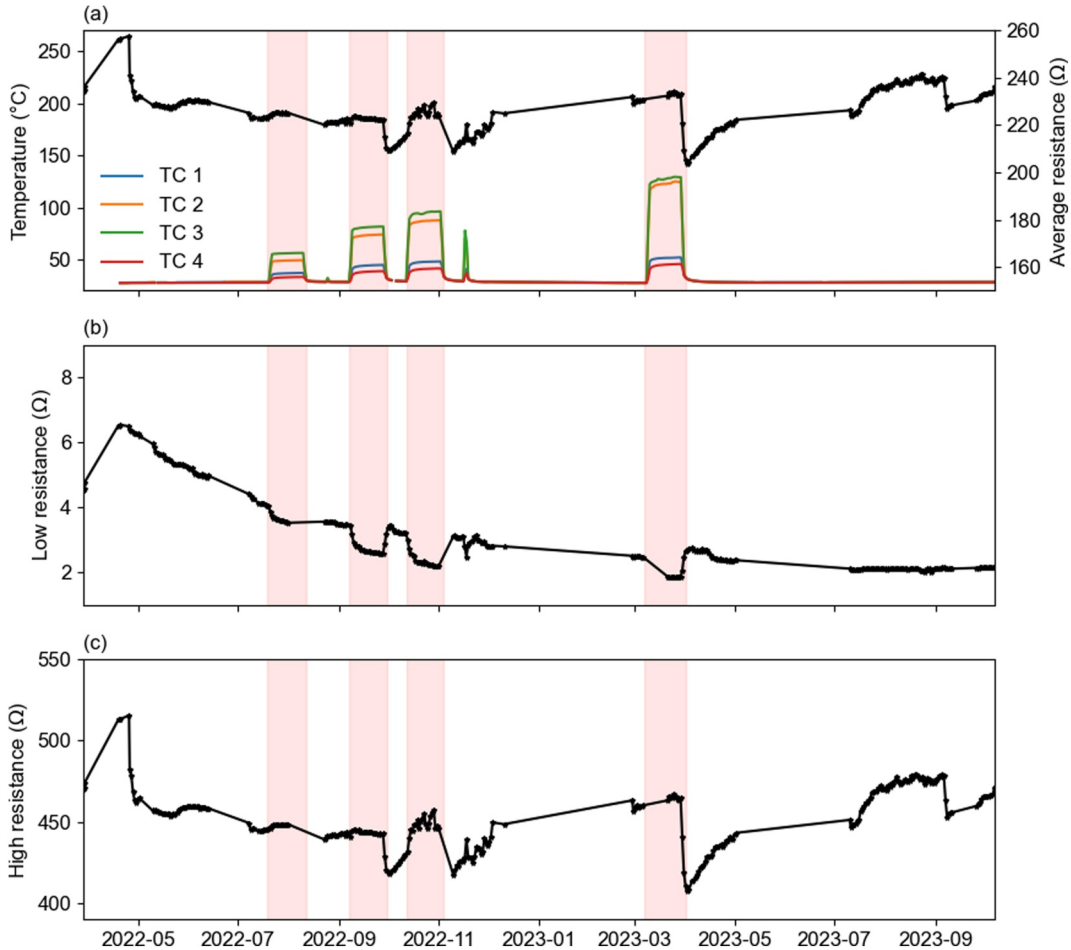


**Figure 2.** Time-series of temperature and average resistance during the BATS2 experiment: (a) daily average temperature data from four thermocouples along the heater and average resistance data from electrical resistivity tomography (ERT), with asterisks indicating the days when ERT data measurements were taken, (b) the trend of low resistance data (<100 Ω) and (c) the trend of high resistance data (≥100 Ω). Red shading represents heating periods.

To obtain 3D resistivity models from measured resistance values, the data must be inverted. However, geophysical inversion problems are often challenging due to their nonlinear, underdetermined, and non-unique nature. To address these complexities, we utilize regularization techniques, incorporating both spatial and temporal smoothing into the inversion objective function (e.g., Kim et al., 2013; Loke et al., 2014). We employed the forward operator from the open-source code PyGIMLi (Rücker et al., 2017) and followed the Gauss-Newton method to iteratively determine the optimal resistivity model (e.g., Chen & Niu, 2022; Günther et al., 2006). However, with a total of hundreds of ERT data sets, it is impractical to ensemble all the data simultaneously for the inversion. For BATS2, we apply a novel windowed 4D inversion algorithm (Wilkinson et al., 2022) to invert the data with spatial and temporal constraints. During the inversion process, data errors were estimated from reciprocal measurements (Slater et al., 2000), with most error magnitudes ranging between 5% and 10%. For the inversion regularization, using large constraints resulted in smoother models, whereas small constraints could lead to overfitting and artifacts. We tested various regularization strengths and found that setting the spatial regularization parameter to 10 and the temporal regularization parameter to 1,000 provided the most optimal and reliable results for our study, as detailed in Text S1 in Supporting Information S1. The inversion process is also highly dependent on the initial model. To address this, we propose a physics-guided initial model specifically designed for this theme, featuring trial initial models that adhere to the physical distribution of EDZ, EdZ, and the far-field area. The details of the inversion methods used in this research are available in Text S1 in Supporting Information S1.

### 2.4. Time-Series Clustering

Applying simple machine learning algorithms to temporal data sets can facilitate the classification of resistivity models into zones that exhibit relatively consistent dynamics over time (Delforge et al., 2021; Watle et al., 2023). The primary objective of clustering is to identify areas potentially affected by rock salt damage or other processes of interest. For instance, THM processes vary across different rock salt regions due to distinct physical properties. This variation leads to different resistivity changes during the heating and cooling phases and thus we can employ clustering techniques to group areas with similar characteristics. In this study, our focus is primarily on data trends. We normalize data variations using the Z-score and then apply Cosine similarity with the K-means algorithm for clustering (Arthur & Vassilvitskii, 2007). Both Z-score normalization and Cosine similarity are designed to emphasize the trend rather than the magnitude of the data changes.

## 3. Results

### 3.1. Raw Data Trend

The measured temperature and resistance changes are illustrated in Figure 2. Figure 2a shows a plot of average resistance changes with corresponding temperature changes. The resistance is not adjusted for temperature effects because observing the direct impact of temperature on resistance is one aspect of understanding the THM processes. This figure reveals a notable increase in average resistance during the initial phase, which then returns to baseline levels before the beginning of the first heating phase. This is also observed in the BATS1 test (K. Kuhlman et al., 2021). These initial changes in resistance can be attributed to brine drainage and rock disturbance following excavation (K. L. Kuhlman & Malama, 2013), with resistance returning to baseline due to the re-establishment of brine equilibrium. Interestingly, during the heating phases, the average resistance first increases and then decreases sharply immediately after heating, which is evident from the data immediately following the second and fourth heating phases. This observation might seem counterintuitive since an increase in temperature typically results in a decrease in resistivity in geomaterials (Hayley et al., 2007).

To investigate the counterintuitive changes, we conducted a detailed analysis of Figure 2a, categorizing the resistance values into two groups: low resistance ($<100\ \Omega$) and high resistance ($\geq 100\ \Omega$). These groups are illustrated in Figures 2b and 2c, respectively. During the heating phases, it was observed that the higher resistance increased, whereas the lower resistance decreased. After heating, the trend reversed, with the higher resistance values decreasing and the lower resistances increasing. This finding suggests that the thermal effects on resistivity within the monitoring area are heterogeneous. To gain preliminary insights into these heterogeneous responses, we plotted the electrode locations for both high and low resistances. An example of this is shown in Figure S1 in Supporting Information S1. From the electrode locations, we observed that most of the low resistances were measured by electrodes positioned across the heater (Figure S1a in Supporting Information S1), while most high resistances were recorded by electrodes situated along the rock salt edges (Figure S1b in Supporting Information S1). This observation may indicate that the heterogeneous processes occur in distinct areas, depending on their distance to the heater excavation hole.

### 3.2. Baseline Resistivity Images

Following the ERT data process and inversion procedure as described, we inverted all the measured ERT data using the advanced inversion algorithm. In this study, we focus more on discussing the inverted results from the second heating phase because the ERT data was fully measured before, during, and after heating in this period, while for the other heating phases, there were data gaps due to equipment failures or power outages. This comprehensive data coverage allows us to gain a detailed understanding of the entire THM process during the second heating phase.

We first show the resistivity distribution of the selected baseline (2022/08/30) before heating Phase 2. The overall 3D resistivity model at normal temperature (~25°C) in Figure 3a indicates a central low-resistivity zone surrounded by a high-resistivity area, except for the area near $Z = -4$ to $-5$ m (the back of the heater borehole). Figure 3b shows the heterogeneous resistivity distribution along the borehole. Notably, a low-resistivity zone (e.g., Point 3: 36 Ω·m) is roughly distributed around −0.5–0.5 m in the X direction and 0 to −6 m in the Z direction, which is likely caused by the drift excavation damage. Within this central low-resistivity zone, an extra-low resistivity zone (e.g., Point 4: 11 Ω·m) is observed behind the heater borehole at $Z > -3.66$ m. This could be

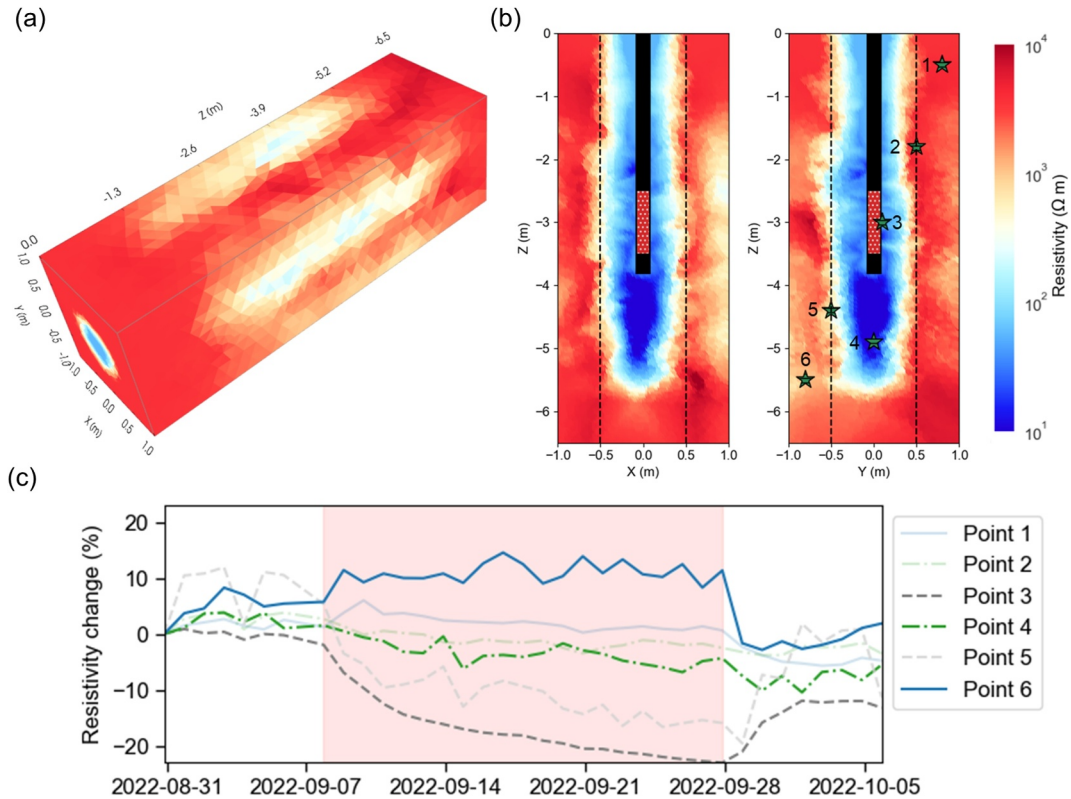


**Figure 3.** The inverted resistivity distribution from the selected baseline (2022/08/30) in heating Phase 2: (a) a 3D perspective, (b) cross-sections along heater borehole with the extent of heated borehole and heater and the locations of selected points; the black and red rectangles are Heater borehole and the heater, and (c) the resistivity changes at the six points shown in panel (b) during second heating phase; note that the lines with same trend is in the same color and line style, one of them is faded to make figure clearer and detailed changes can be found in Figure S3 in Supporting Information S1.

attributed to the post-excavation movement of brine into the damaged zone, driven by gravity and surrounded by the lower porosity area. The surrounding areas are mostly high resistivity (e.g., Point 1: 4,329 Ω·m and Point 6: 1,247 Ω·m), revealing the relatively intact rock salt. The resistivity at the interface between the low and high resistivity zones varies (e.g., Point 2: 2297 Ω·m and Point 5: 291 Ω·m). The cross-sections in Figure S2 in Supporting Information S1 show similar features as in the 3D perspective, and the low-resistivity zone and heterogeneity are larger when closer to the bottom of the heater drift. This indicates that drift excavation introduces heterogeneous damage to the rock salt, which needs to be considered in long-term safety modeling.

Long-term THM modeling relies on the parametrization of initial conditions. Resistivity can be utilized to estimate the porosity and water content of the subsurface according to Archie's law (Archie, 1942):

$$\rho = \rho_{\mathrm{w}} \phi^{-m} S^{-n} = \rho_{\mathrm{w}} \theta^{-m} S^{m-n} \tag{1}$$

where $\rho_w$ is the pore water (brine) resistivity, $\phi$ is the porosity, $m$ is the porosity exponent, $S$ is the degree of saturation, $n$ is the saturation exponent, and $\theta$ is the volumetric water content. Laboratory tests on rock salt (Yaramanci, 1994, 2000) suggest $\rho_{\mathrm{w}} = 0.035$ Ω·m, $m = 1.9$ and $m–n \approx 0$. Using Equation 1, we can estimate the subsurface's water content through resistivity values. For instance, in the low resistivity zone, Points 3 and 4 are estimated to have water contents of 2.6% and 4.8%, respectively. In contrast, the selected points in the high resistivity zone, Points 1 and 6, are estimated to have water contents of 0.2% and 0.4%, respectively. Meanwhile, the selected interface points, Points 2 and 5, are estimated to have water contents of 0.3% and 0.9%, respectively. These estimations reveal that the water content near the heater borehole is significantly higher, likely due to excavation damage and brine migration, especially in the extra-low resistivity zone (near Point 4) which is surrounded by a high resistivity zone and could have a water content around 5%. However, the porosity around the

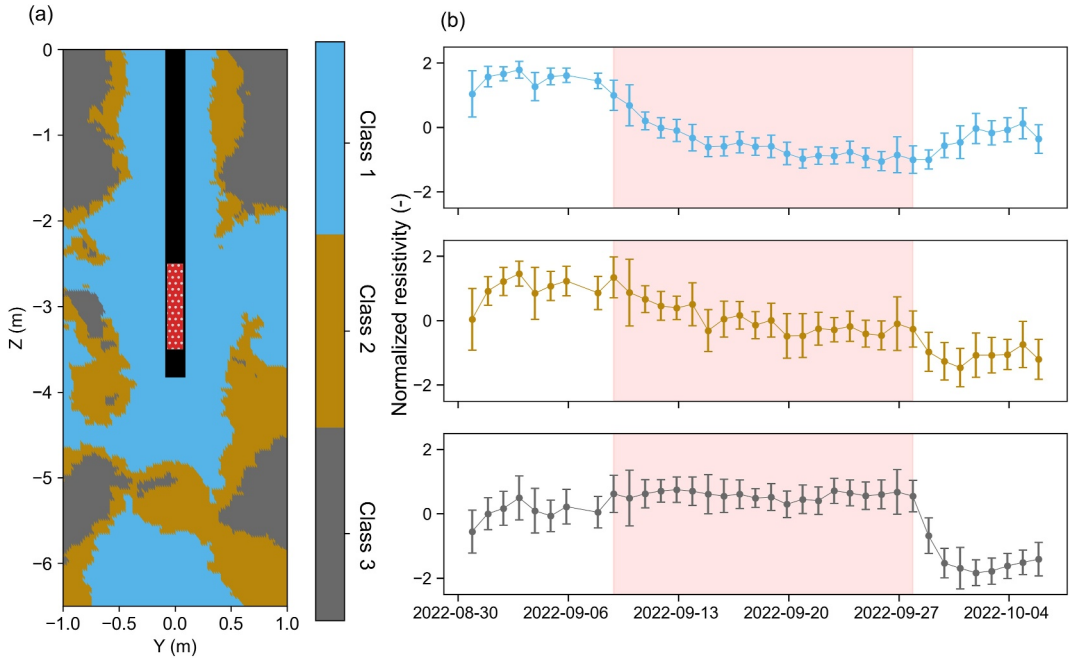


**Figure 4.** The time-series clustering results: (a) the spatial distribution of classes with heater borehole and heated interval indicated, and (b) the normalized resistivity changes in each cluster with its uncertainty (one standard deviation). Red shading represents heating periods.

damaged zone could be very large (~10%), indicating it is likely still unsaturated. From the center of the heater borehole to its edge, the water content decreases significantly to around 0.2%, indicating a reduction of more than two orders of magnitude. As demonstrated by tests on rock salt in Asse, North Germany (Yaramanci, 2000), the porosity of undisturbed rock is approximately 0.1%–0.5%, suggesting that the high resistivity parts in this study are almost saturated rock salt.

### 3.3. Temporal Resistivity Changes

The analysis of temporal resistivity changes reveals significant insights into the subsurface THM processes during and after the heating phase. The temporal resistivity changes across Points 1 to 6 are illustrated in Figure 3c and detailed in Figure S3 in Supporting Information S1. Most points (Points 2 to 5), within low resistivity or transition zones, show a decreasing trend during heating, while the points (Points 1 and 6) at the edge exhibit a general increasing trend during this period. These resistivity changes during heating are very consistent with the discussion of raw resistance presented in Figure 2. After heating, the resistivity changes become more complex. Among the points whose resistivity decreases during heating, Points 3 and 5 show increasing trends after heating, whereas Points 2 and 4 continue to show a decreasing trend. Similarly, Points 1 and 6 also exhibit a decreasing trend after heating.

The resistivity changes highlight the heterogeneous THM processes occurring at different locations. Overall, these changes can be categorized into three classes: Class 1 (e.g., Points 3 and 5), which shows a decrease in resistivity during heating followed by an increase after heating; Class 2 (e.g., Points 2 and 4), which experiences a decrease both during and after heating; and Class 3 (e.g., Points 1 and 6), where resistivity increases during heating but decreases afterward. By applying time-series clustering to the resistivity changes during the second heating phase, we have mapped the spatial distribution of these three classes, as shown in Figure 4a, with the corresponding normalized resistivity changes for each class presented in Figure 4b. By combining the locations of different classes with features of resistivity change, we can infer the THM processes occurring in various areas. For example, Class 1, encompassing most of the area near the heater, exhibits decreased resistivity during heating as the increased temperature enhances the mobility of ions in brine. The varied decreasing trends in different locations (e.g., Points 2 to 5) suggest that thermal gradients influence fluid mobility. After heating, as the temperature effect disappears, resistivity tends to increase. Class 2, covering most of the area between the heater and

the surrounding borders, shows a continuous decrease in resistivity after heating, likely due to mechanical changes, for example, new fracture generation or extension of existing fractures, induced by thermal expansion, which does not fully recover post-heating. The mechanical changes are also evident in the fiber optic measurement data, which show significant strain increasing near point 4 even after heating (Figure S5a in Supporting Information S1). Class 3, mostly located in corner areas, presents an unusual increase in resistivity during heating. Our explanation for this is that thermal expansion in the center part compresses the surroundings, where more intact rock salt exists. This compression decreases porosity and permeability (Blankenship & Stickney, 1983). Particularly in high resistivity zones, where original porosity is minimal, even a slight reduction in porosity can cause a significant increase in resistivity, due to the high compressibility of fractures. After heating, as compression diminishes, resistivity decreases rapidly. Interestingly, after heating, none of the classes return to their baseline resistivity levels, remaining lower than the baseline, but the temperature returns to the pre-heating level. This could be due to increased permeability due to thermal contraction during cooling, facilitating brine migration into the drifts (Tounsi et al., 2023), a phenomenon observed during BATS and other similar previous experiments. The brine production rate data also support this brine migration as in Figure S6 and details in Text S2 in Supporting Information S1.

## 4. Discussion

This section discusses how 4D ERT results may improve long-term performance assessment modeling, which depends on the accurate representation of physical processes and the parameterization of initial conditions. Initial condition parameterization often requires spatial information on porosity and moisture (Rutqvist, 2017), which can be estimated from resistivity data through additional in situ experiments and laboratory tests. For instance, moisture content has been estimated using Equation 1, and with in situ saturation tests, porosity can also be inferred. All estimations in this work are based on the petrophysical model of rock salt from another site, and the potential bias can be mitigated by further laboratory testing with samples from the BATS2 test.

The representation of physical processes, including coupled processes, boundary conditions, and spatial variability, varies in modeling, particularly between the damaged zone and the far-field zone (e.g., Blanco-Martín et al., 2018). In the damaged zone, tight coupling is essential to accommodate the significant interactions between processes and the complex boundary conditions reflecting the immediate impacts of excavation. In the far field, simpler coupling mechanisms and boundary conditions may be adequate. Our time-series clustering results can help us infer the representation of physical processes in different areas. For example, Class 1 acts like a porous medium with enhanced mobility of ions with increased temperature, indicating that Class 1 is where the salt is fractured enough for porosity to be less compressible. Similarly, there are also fractures in Class 2, but post-heating resistivity decreases indicate that heating may induce more fractures here, suggesting that Class 2 is an area where there are a few discrete fractures, perhaps not quite a porous medium. Class 3 is mostly affected by the compressibility of fractures, suggesting that Class 3 is an area where fractures are sparse, porosity is very compressible, and the region is mainly affected by mechanical changes.

Our results in Class 1 can also be further evaluated for consistency with the former findings in BATS1 (Wang et al., 2023), where the monitoring systems covered a smaller area, mostly over the damaged zone. In BATS1, the resistivity data only showed decreases during heating and increases after heating, which is the same feature observed in Class 1. Moreover, the brine migration induced by thermal pressurization from hotter to colder areas, as revealed by discrete element modeling in BATS1, is also evident in Class 1. For instance, although the temperature difference between TC3 and TC4 reached up to 40°C, the resistivity decreases differed by only 5% in these two areas. The temperature difference alone cannot explain the discrepancy in resistivity change (e.g., 2% temperature coefficient from Hayley et al., 2007), and the concept of thermally-driven brine migration can explain the significant resistivity decrease in the colder area (TC4). Overall, we suggest that Classes 1 and 2, representing the EDZ/EdZ, require a more complex representation of physical processes, while Class 3 can be considered as the far field and assigned as intact rock during modeling.

## 5. Conclusions

This study highlights the capability of 4D ERT in unrevealing the complex THM processes within salt formations, key for assessing the long-term safety of nuclear waste repositories. The advanced inversion method and clustering analysis can provide insightful resistivity dynamics in space and time for further analysis. By analyzing

these dynamics of resistivity, we can estimate subsurface properties and identify areas with distinct THM behaviors. This information can improve long-term performance assessment modeling, which relies on accurately representing physical processes and initializing conditions. Overall, this work shows the potential ability of ERT to improve subsurface modeling and safety assessment practices in nuclear waste management.

## Data Availability Statement

The codes, ERT and temperature data are available at Chen and Wu (2024).

**Acknowledgments**
This research was funded by the Department of Energy (DOE) Office of Nuclear Energy Spent Fuel and Waste Science & Technology campaign under the Salt Disposal Research work package with contract number DE-AC02-05CH11231 to Lawrence Berkeley National Laboratory. This paper describes objective technical results and analysis. Any subjective views or opinions that might be expressed in the paper do not necessarily represent the views of the U.S. Department of Energy or the United States Government. This article has been co-authored by an employee of National Technology & Engineering Solutions of Sandia, LLC under Contract No. DE-NA0003525 with the U.S. Department of Energy. The employee owns all right, title and interest in and to the article and is solely responsible for its contents. The United States Government retains and the publisher, by accepting the article for publication, acknowledges that the United States Government retains a non-exclusive, paid-up, irrevocable, world-wide license to publish or reproduce the published form of this article or allow others to do so, for United States Government purposes. The DOE will provide public access to these results of federally sponsored research in accordance with the DOE Public Access Plan https://www.energy.gov/downloads/doe-public-access-plan.

## References

Archie, G. E. (1942). The electrical resistivity log as an aid in determining some reservoir characteristics. *Transactions of the AIME*, *146*(01), 54–62. https://doi.org/10.2118/942054-g

Arthur, D., & Vassilvitskii, S. (2007). k-means++: The advantages of careful seeding. *Soda*, *7*, 1027–1035.

Betters, C., Vornlocher, J., Paronish, T., Crandall, D., Moore, J., & Kuhlman, K. L. (2020). *Computed tomography scanning and geophysical measurements of the Salado formation from boreholes at the waste isolation pilot plant (No. df70467b-fdd9-4567-8614-44abee6da5fa)*. National Energy Technology Laboratory (NETL), Morgantown, WV (United States).

Binley, A., Hubbard, S. S., Huisman, J. A., Revil, A., Robinson, D. A., Singha, K., & Slater, L. D. (2015). The emergence of hydrogeophysics for improved understanding of subsurface processes over multiple scales. *Water Resources Research*, *51*(6), 3837–3866. https://doi.org/10.1002/2015wr017016

Birkholzer, J., Houseworth, J., & Tsang, C. F. (2012). Geologic disposal of high-level radioactive waste: Status, key issues, and trends. *Annual Review of Environment and Resources*, *37*(1), 79–106. https://doi.org/10.1146/annurev-environ-090611-143314

Blanco-Martín, L., Rutqvist, J., Battistelli, A., & Birkholzer, J. T. (2018). Coupled processes modeling in rock salt and crushed salt including halite solubility constraints: Application to disposal of heat-generating nuclear waste. *Transport in Porous Media*, *124*(1), 159–182. https://doi.org/10.1007/s11242-018-1057-7

Blankenship, D. A., & Stickney, R. G. (1983). *Nitrogen gas permeability tests at Avery Island (No. ONWI-190 (3))*. RE/SPEC, Inc.

Chen, H., & Niu, Q. (2022). Improving moisture content estimation from field resistivity measurements with subsurface structure information. *Journal of Hydrology*, *613*, 128343. https://doi.org/10.1016/j.jhydrol.2022.128343

Chen, H., & Wu, Y. (2024). WIPP_BATS2_Temperature_resistivity [Dataset]. *Zenodo*. https://doi.org/10.5281/zenodo.10910112

Cosenza, P., Ghoreychi, M., Bazargan-Sabet, B., & De Marsily, G. (1999). In situ rock salt permeability measurement for long term safety assessment of storage. *International Journal of Rock Mechanics and Mining Sciences*, *36*(4), 509–526. https://doi.org/10.1016/s0148-9062(99)00017-0

Delforge, D., Watlet, A., Kaufmann, O., Van Camp, M., & Vanclooster, M. (2021). Time-series clustering approaches for subsurface zonation and hydrofacies detection using a real time-lapse electrical resistivity dataset. *Journal of Applied Geophysics*, *184*, 104203. https://doi.org/10.1016/j.jappgeo.2020.104203

Günther, R. M., Salzer, K., Popp, T., & Lüdeling, C. (2015). Steady-state creep of rock salt: Improved approaches for lab determination and modelling. *Rock Mechanics and Rock Engineering*, *48*(6), 2603–2613. https://doi.org/10.1007/s00603-015-0839-2

Günther, T., Rücker, C., & Spitzer, K. (2006). Three-dimensional modelling and inversion of DC resistivity data incorporating topography—II. Inversion. *Geophysical Journal International*, *166*(2), 506–517. https://doi.org/10.1111/j.1365-246x.2006.03011.x

Hayley, K., Bentley, L. R., Gharibi, M., & Nightingale, M. (2007). Low temperature dependence of electrical resistivity: Implications for near surface geophysical monitoring. *Geophysical Research Letters*, *34*(18). https://doi.org/10.1029/2007gl031124

Hovorka, S. D. (1997). Quaternary evolution of ephemeral playa lakes on the Southern high plains of Texas, USA: Cyclic variation in lake level recorded in sediments. *Journal of Paleolimnology*, *17*(1), 131–146. https://doi.org/10.1023/a:1007998902734

Hu, M., Steefel, C. I., & Rutqvist, J. (2021). Microscale mechanical-chemical modeling of granular salt: Insights for creep. *Journal of Geophysical Research: Solid Earth*, *126*(12), e2021JB023112. https://doi.org/10.1029/2021jb023112

Kim, J. H., Supper, R., Tsourlos, P., & Yi, M. J. (2013). Four-dimensional inversion of resistivity monitoring data through LP norm minimizations. *Geophysical Journal International*, *195*(3), 1640–1656. https://doi.org/10.1093/gji/ggt324

Kruschwitz, S., & Yaramanci, U. (2004). Detection and characterization of the disturbed rock zone in claystone with the complex resistivity method. *Journal of Applied Geophysics*, *57*(1), 63–79. https://doi.org/10.1016/j.jappgeo.2004.09.003

Kuhlman, K., Mills, M., Jayne, R., Matteo, E., Herrick, C., Nemer, M., et al. (2021). *Brine availability test in salt (BATS) FY21 update (No. SAND2021-10962R)*. Sandia National Laboratories.

Kuhlman, K., Mills, M., Jayne, R., Matteo, E., Herrick, C., Nemer, M., et al. (2023). *Brine availability test in salt (BATS) FY23 update (No. SAND2023-08820R)*. Sandia National Laboratories.

Kuhlman, K. L., & Malama, B. (2013). *Brine flow in heated geologic salt (No. SAND2013-1944)*. Sandia National Laboratories.

Kuhlman, K. L., Mills, M. M., & Matteo, E. N. (2017). *Consensus on intermediate scale salt field test design (No. SAND2017-3179R)*. Sandia National Laboratories.

Loke, M. H., Dahlin, T., & Rucker, D. F. (2014). Smoothness-constrained time-lapse inversion of data from 3D resistivity surveys. *Near Surface Geophysics*, *12*(1), 5–24. https://doi.org/10.3997/1873-0604.2013025

Mathew, M. D. (2022). Nuclear energy: A pathway towards mitigation of global warming. *Progress in Nuclear Energy*, *143*, 1. https://doi.org/10.1016/j.pnucene.2021.104080

McTigue, D. F., & Nowak, E. J. (1987). *Brine transport studies in the bedded salt of the waste isolation pilot plant (WIPP) (No. SAND-87-1274C; CONF-871124-19)*. Sandia National Laboratories.

Rücker, C., Günther, T., & Wagner, F. M. (2017). pyGIMLi: An open-source library for modelling and inversion in geophysics. *Computers & Geosciences*, *109*, 106–123. https://doi.org/10.1016/j.cageo.2017.07.011

Rutqvist, J. (2017). An overview of TOUGH-based geomechanics models. *Computers & Geosciences*, *108*, 56–63. https://doi.org/10.1016/j.cageo.2016.09.007

Schröder, J., Rossignol, N., & Van Oudheusden, M. (2016). Safety in long term radioactive waste management: Insight and oversight. *Safety Science*, *85*, 258–265. https://doi.org/10.1016/j.ssci.2016.02.003

Slater, L., Binley, A. M., Daily, W., & Johnson, R. (2000). Cross-hole electrical imaging of a controlled saline tracer injection. *Journal of Applied Geophysics*, *44*(2–3), 85–102. https://doi.org/10.1016/s0926-9851(00)00002-1

Sweet, J. N., & McCreight, J. E. (1983). Thermal conductivity of rock salt and other geologic materials from the site of the proposed waste isolation pilot plant. In *Thermal conductivity* (Vol. 16, pp. 61–78). Springer US. https://doi.org/10.1007/978-1-4684-4265-6_7

Tounsi, H., Rutqvist, J., Hu, M., & Wolters, R. (2023). Numerical investigation of heating and cooling-induced damage and brine migration in geologic rock salt: Insights from coupled THM modeling of a controlled block scale experiment. *Computers and Geotechnics*, *154*, 105161. https://doi.org/10.1016/j.compgeo.2022.105161

Tsang, C. F., Bernier, F., & Davies, C. (2005). Geohydromechanical processes in the excavation damaged zone in crystalline rock, rock salt, and indurated and plastic clays—In the context of radioactive waste disposal. *International Journal of Rock Mechanics and Mining Sciences*, *42*(1), 109–125. https://doi.org/10.1016/j.ijrmms.2004.08.003

Wang, J., Uhlemann, S., Otto, S., Dozier, B., Kuhlman, K. L., & Wu, Y. (2023). Joint geophysical and numerical insights of the coupled thermal-hydro-mechanical processes during heating in salt. *Journal of Geophysical Research: Solid Earth*, *128*(9), e2023JB026954. https://doi.org/10.1029/2023jb026954

Watlet, A., Thirugnanam, H., Singh, B., Kumar M, N., Brahmanandan, D., Inauen, C., et al. (2023). 4D Electrical resistivity to monitor unstable slopes in mountainous tropical regions: An example from Munnar, India. *Landslides*, *20*(5), 1031–1044. https://doi.org/10.1007/s10346-023-02029-3

Wilkinson, A. J., Randall, E. W., Long, T. M., & Collins, A. (2006). The design of an ERT system for 3D data acquisition and a quantitative evaluation of its performance. *Measurement Science and Technology*, *17*(8), 2088–2096. https://doi.org/10.1088/0957-0233/17/8/006

Wilkinson, P. B., Chambers, J. E., Meldrum, P. I., Kuras, O., Inauen, C. M., Swift, R. T., et al. (2022). Windowed 4D inversion for near real-time geoelectrical monitoring applications. *Frontiers in Earth Science*, *10*, 983603. https://doi.org/10.3389/feart.2022.983603

Yaramanci, U. (1994). Relation of in situ resistivity to water content in salt rocks 1. *Geophysical Prospecting*, *42*(3), 229–239. https://doi.org/10.1111/j.1365-2478.1994.tb00207.x

Yaramanci, U. (2000). Geoelectric exploration and monitoring in rock salt for the safety assessment of underground waste disposal sites. *Journal of Applied Geophysics*, *44*(2–3), 181–196. https://doi.org/10.1016/s0926-9851(99)00013-0

## References From the Supporting Information

Bechthold, W., Heusermann, S., & Smailos, E. (2004). *Backfilling and sealing of underground respositories for radioactive waste in salt: Bambus II project*. Publications Office of the European Union.

Bhattacharya, P. (2012). *Direct current geoelectric sounding: Principles and interpretation*. Elsevier.

Constable, S. (2010). Ten years of marine CSEM for hydrocarbon exploration. *Geophysics*, *75*(5), 75A67–75A81. https://doi.org/10.1190/1.3483451

Jockwer, N., & Wieczorek, K. (2008). ADDIGAS. Advective and diffusive gas transport in rock salt formations. *Gesellschaft fuer Anlagen-und Reaktorsicherheit mbH (GRS)*.

Oldenburg, D. W., & Pratt, D. A. (2007). Geophysical inversion for mineral exploration: A decade of progress in theory and practice. In *Proceedings of exploration* (Vol. 7, pp. 61–95).